ISSN 1023-1935, Russian Journal of Electrochemistry, 2018, Vol. 54, No. 12, pp. 1176–1185. © Pleiades Publishing, Ltd., 2018.
Original Russian Text © V.V. Vashook, J. Zosel, M. Schelter, E. Sperling, J. Posseckardt, L.O. Vasylechko, I.V. Matsukevich, N.P. Krutko, U. Guth, M. Mertig, 2018, published in Elektrokhimiya, 2018, Vol. 54, No. 12, pp. 1124–1134.

Nanocomposite Ceramics on the Basis of Magnesium, Cerium, and Samarium Oxides

V. V. Vashook[a, b, *], J. Zosel[b], M. Schelter[b], E. Sperling[c], J. Posseckardt[b], L. O. Vasylechko[d], I. V. Matsukevich[a, **], N. P. Krutko[a], U. Guth[b], and M. Mertig[b]

[a] *Institute of General and Inorganic Chemistry, National Academy of Sciences of Belarus, Minsk, 220072 Belarus*
[b] *Kurt-Schwabe-Institut für Mess- und Sensortechnik e.V. Meinsberg, Waldheim, 04736 Germany*
[c] *Technische Universität Dresden, Institute of Physical Chemistry, Dresden, 01069 Germany*
[d] *Lviv Polytechnic National University, Lviv, 79013 Ukraine*
**e-mail: vladimir_vashook@yahoo.com*
***e-mail: irinavas.k1975@gmail.com*

Received June 21, 2017; in final form, December 25, 2017

Abstract—A model of conductivity of nanocomposite ceramics consisting of solid-electrolyte and dielectric phases is proposed based on the assumption that the conductivity of grain boundaries between the solid-electrolyte and dielectric phases is higher than the conductivity of the volume of particles in the solid-electrolyte phase and its grain boundaries. Taking into account the size of particles, the thickness of grain boundaries, and the bulk and grain-boundary conductivities, the grain size of composite ceramics for which the conductivity may exceed the conductivity of single-phase solid-electrolyte ceramics is assessed. For testing this model, the composite samples are synthesized based on dielectric magnesium oxide and solid-electrolyte cerium oxide doped with samarium oxide. It is shown that introduction of 50 mol % magnesium oxide into composite ceramics has virtually no effect on its conductivity as compared with single-phase solid-electrolyte ceramics. This result can be explained by assuming the appearance of accelerated transport routes for oxygen ions in grain boundaries between dielectric and solid-electrolyte phases. Further dispersion, optimization of the ratio, and increase in distribution homogeneity of components can confirm the validity of the proposed conductivity model and open up the possibility of preparation of oxide solid-electrolyte materials with higher conductivity.

Keywords: oxide solid electrolyte materials, nanocomposite ceramics, magnesium oxide, cerium oxide, microstructure, thermal expansion, electrical conductivity

DOI: 10.1134/S1023193518140100

INTRODUCTION

The development of composite solid electrolytes is one of the directions for the development of new highly conductive solid-electrolyte materials [1–4]. The phenomenon of the increase in ionic conductivity of a ionic compound upon the addition of an inert oxide was first observed in [5] after mixing lithium iodide with aluminum oxide. Since this discovery, quite a number of composite materials with higher ionic conductivity as compared with single-phase materials were developed. The widest quest for composite solid-electrolyte materials was carried out among the cation-conducting ionic salts of lithium [5–8], silver [9], and copper [10], as well as for anion-conducting salts with the fluorite structure such as CaF_2 [11–13]. The higher conductivity of composite materials as compared with single-phase solid electrolytes was also observed in certain other systems: Na_2CO_3/Na_2SO_4 [14–16], $Ba(NO_3)_2$–Al_2O_3 [17]. Only a small number of studies were devoted to composite materials with oxygen-ion conduction $Ce_{1-x}Sm_xO_{2-x/2}/Na_2CO_3$ [18].

To obtain composite solid electrolytes, the oxides of aluminum, silicon, cerium, iron, molybdenum, tungsten, tin, samarium, calcium, etc. were taken as the inert additives. It was experimentally found that the size of added particles should not exceed 1–10 μm [4].

The main parameters determining the ionic conductivity of composite electrolytes are the conductivity and the relative content of each individual phase (component), the morphology of individual phases, and characteristics of all possible grain boundaries in the composite. According to authors of [2], depending on the spatial arrangement and concentration of one of components, the composite electrolytes can be divided into the following four groups: structures with closed inclusions, structures with interpenetrating components, structures combining the former two types, and statistical mixtures.

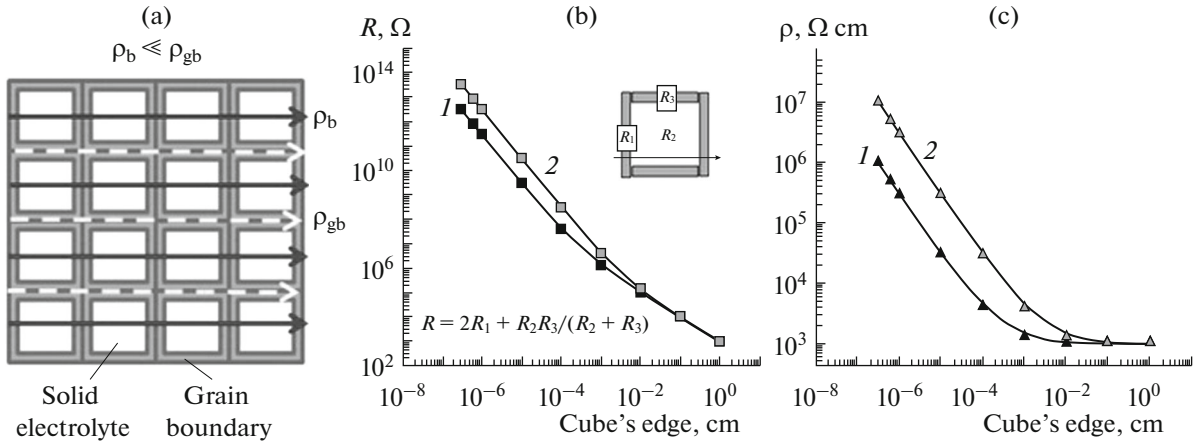

Fig. 1. (a) Illustration of the microstructure of idealized single-phase ceramic materials and (b) resistance, and (c) resistivity of individual cubic grain: (*1*) $\rho_b/\rho_{gb} = 0.001$; (*2*) $\rho_b/\rho_{gb} = 0.0001$.

The conductivity of components may change by orders of magnitude depending on many factors. To interpret the ionic conductivity of components, several models were proposed such as the model of electric double layer, the efficient environment models, the percolation theory models, which are described in detail in monograph [2]. According to the author of monograph [4], no reliable methods for calculating conductivity of composite solid electrolytes were developed to the time of its publication. All existing theoretical equations are either limited to the region of low concentrations or too complicated to be analyzed and used in practice.

The grain boundaries of single-phase ceramics conducting due to oxygen ions usually have the higher resistivity as compared with grain's volume [1, 19, 20]. However, quite different situation may arise in composite materials consisting of solid-electrolyte and dielectric phases. Thus, it was found that epitaxial films of yttrium-stabilized zirconia (YSZ) formed on MgO single crystals at temperatures of 600–800°C demonstrate the 3–4 orders of magnitude higher conductivity as compared with YSZ [21]. Moreover, an interphase layer with the thickness of 1.6 nm was observed to form between YSZ and MgO phases.

The higher oxygen-ion conductivity of such components as compared with single-phase solid electrolytes can be realized in certain ceramic structures for certain parameters of conductivity of individual components.

If we assume that the single-phase solid-electrolyte material SE consists of cubic grains with the edge a, the grain boundary thickness d (Fig. 1a), and the resistivity of grain boundaries (ρ_{gb}) higher than resistivity of grain's bulk (ρ_b), the resistance (R_{sc}) of individual cubes and the resistivity of this ceramic material (ρ_{sm}) can be calculated with the use of the following equations:

$$R_{sc} = 2R_1 + \frac{R_2R_3}{R_2 + R_3}, \quad (1)$$

$$\rho_{sm} = R_{sc}a, \quad (2)$$

where R_1 is the resistance of grain boundaries oriented normally to the current direction, R_2 is the bulk resistance of solid-electrolyte grains, R_3 is the resistance of grain boundaries oriented in parallel to the current direction. Figures 1b and 1c illustrate the resistance of individual cubic grains and the resistivity of material built of such grains as a function of the particle size and under assumption that $d = 1.5$ nm, $\rho_b = 1$ kΩ cm, and $\rho_{gb} = 1$ or 10 MΩ cm. As the grain size decreases, their resistance increases along with the resistivity of material. The stronger increase is observed with the increase in the ratio ρ_{gb}/ρ_b.

Quite different situation arises in a two-phase composite material which consists of solid-electrolyte and dielectric phases. If the grains of both components in the composite are cubes, have equal size, and are ideally mixed and adjusted to one another (Fig. 2a), then the resistance of two cubes connected in parallel (R_{cc}) and the resistivity of the composite material (ρ_{cm}) based on such cubic grains can be expressed as follows:

$$R_{cc} = R_1 + \frac{R_2R_3R_4}{R_2R_3 + R_3R_4 + R_2R_4}, \quad (3)$$

$$\rho_{cm} = R_{cc}2a, \quad (4)$$

where R_4 is the resistance of the dielectric phase; the other designations are the same.

Figure 2b illustrates the changes in the resistance (R_{cc}) of two cubic grains connected in parallel as a function of cube's edge. Figure 2c shows the change in the resistivity (ρ_{cm}) of composite material based on these components under the condition that the resis-

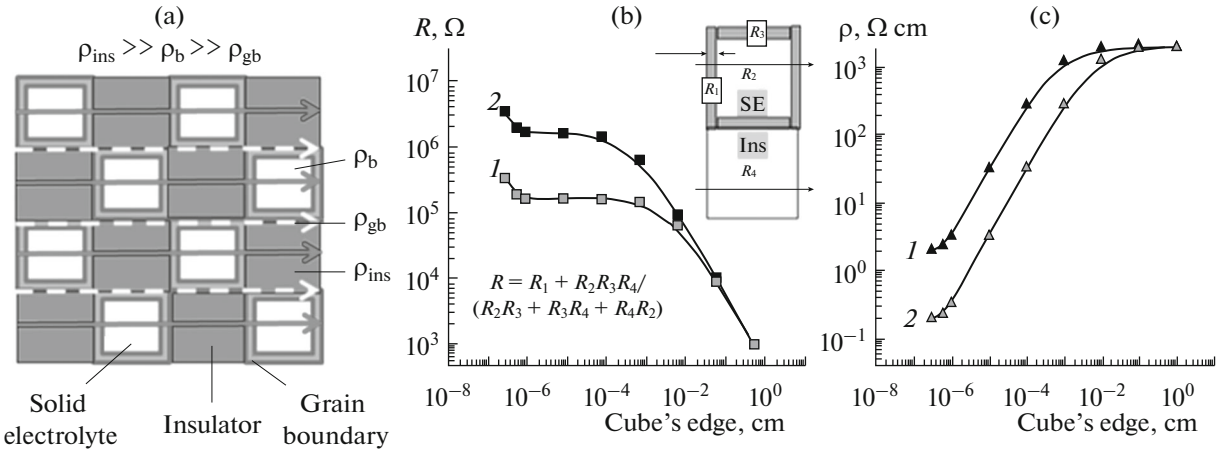

Fig. 2. (a) Illustration of the microstructure of idealized two-phase ceramic material and (b) resistance and (c) resistivity of two adjacent cubic grains: (*1*) $\rho_b/\rho_{gb} = 0.001$; (*2*) $\rho_b/\rho_{gb} = 0.0001$.

tivity of grain boundaries (ρ_{gb}) is lower than the resistivity of electrolyte (ρ_{bc}). For instance, this situation is observed in the MgO–YSZ system [21]. It is assumed that the thickness of grain boundaries is 1.5 nm, the bulk resistivity of solid-electrolyte grains $\rho_{se} = 1$ kΩ cm, the bulk resistivity of the insulator grains $\rho_{ins} = 1$ MΩ cm, and the resistivity of grain boundaries $\rho_{gb} = 0.1$ and 1 Ω cm. The decrease in the particle size of composite material from 10 μm to 10 nm at the fixed resistivities of components and the constant thickness of grain boundaries is accompanied by the decrease in resistivity of composite material by 2.5 orders of magnitude. The increase in the ρ_b/ρ_{gb} ratio and the grain-boundary thickness leads to the stronger relative decrease in composite resistivity. Modeling clearly shows that for the fixed resistivity and size of particles, the resistivity of the nanocomposite material may be considerably higher as compared with single-phase solid-electrolyte material.

In this study, to confirm the mentioned conductivity model of composite ceramics, we used the methods of joint grinding and supersonication in various liquid media to obtain nanocomposite powders (SDC + MgO) based on MgO nanopowder as the insulator phase and $Ce_{0.8}Sm_{0.2}O_{1.9-\delta}$ (SDC) nanopowder as the solid-electrolyte phase. Analogous nanocomposite powders were also obtained by the method of self-propagating high-temperature synthesis (SHS) [22] from glycine-citrate-nitrate mixtures. Based on these powders, we obtained nanocomposite ceramics and studied their microstructure, thermal expansion, and electrical conductivity as a function of homogeneity and particle size of nanopowders.

EXPERIMENTAL

SDC nanopowder was synthesized by SHS method from glycine-citrate-nitrate mixtures as described in [23–26]. As the starting materials, we used ammonium–cerium nitrate $(NH_4)_2Ce(NO_3)_6$ (>99.5%, Alfa Aesar), samarium nitrate $Sm(NO_3)_3 \cdot 6H_2O$ (99.9%, Alfa Aesar), citric acid monohydrate $C_6H_8O_7 \cdot H_2O$ (99%, Alfa Aesar), and glycine NH_2CH_2COOH (100%, Riedel de Haen). The required amounts of aqueous solutions of metal nitrates were mixed with necessary amounts of glycine and citric acid in the molar ratio of carbon to nitrogen equal to 0.3, to ensure controlled combustion [27]. The resulting solution was evaporated on a hot plate at 300°C on constant stirring. In the course of evaporation, the solution thickened and transformed into gel. The gel transformed into caramel, then foamed, and, finely, inflamed in a single point. The burning front propagated in several seconds over the whole mass of the foamed semiproduct. As a result of burning, light-brown powder was formed which after 1 h thermal treatment in air at 300°C transformed into white powder.

To obtain nanocomposite powders, the synthesized SDC nanopowder was mixed in the planetary mill Pulverisette 7 (Fritsch, Germany) or in the supersonic mixer UIS250 (Hielscher, Germany) with MgO nanopowder (Chempur, pureness >99.5%, particle size 36 nm, specific surface 46 m^2/g) in the molar ratio 1 : 1 in water or ethanol. Nanocomposite powders were also synthesized by the glycine–citrate–nitrate method by introducing magnesium-containing compounds such as as MgO or $Mg(NO_3)_2$ into reaction mixture [23].

The resulting (SDC + MgO) powders were pressed into cuboids with the size (10 × 3 × 1.5 mm^3) under pressure of about 5000 N/cm^2 and sintered in air at 1500–1600°C for 5 h.

The precision X-ray diffraction analysis of nanocomposite powders was carried out at room temperature by means of Huber Image Plate Guinier diffractometer G670 (Huber, Germany), and also diffrac-

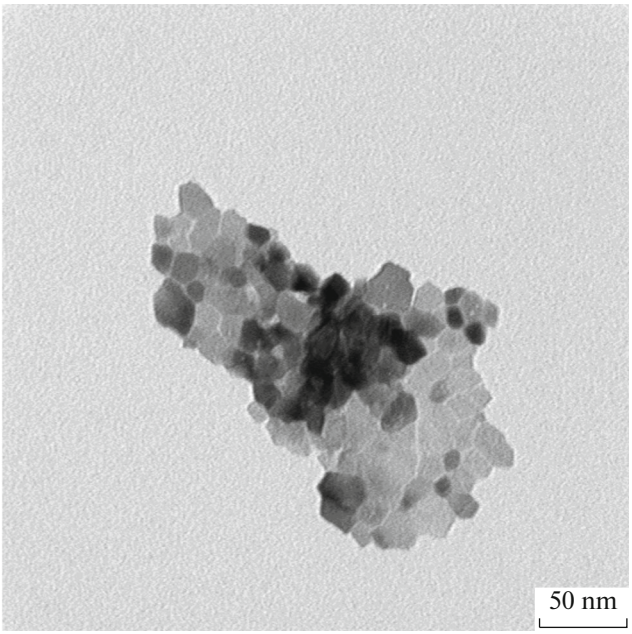

Fig. 3. TEM image of SDC particles synthesized by high-temperature self-propagating combustion and treated in air at 300°C for 30 min.

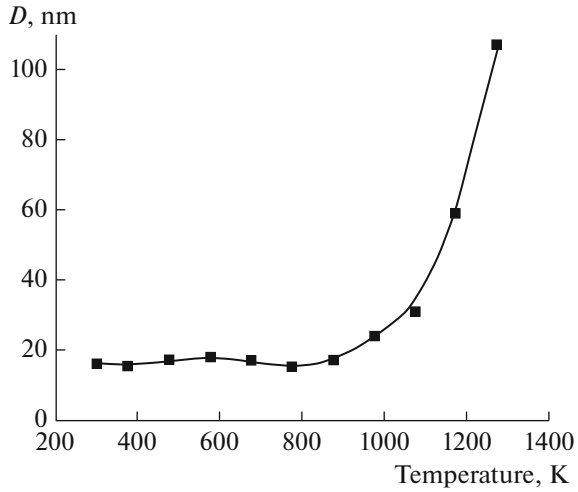

Fig. 4. Temperature dependence of the average grain size of $Ce_{0.8}Sm_{0.2}O_{1.9-\delta}$ powder, found by the method of Williamson–Hall [28].

tometer Bruker D8 Discover (Bruker, Germany) equipped with high-temperature chamber. The specific surface was determined by the BET method on setup Beckman Coulter 3100 (Beckman, Germany). Powders were placed into a standard measuring vessel and preheated for 1 h at 250°C in vacuum. Nitrogen was used as the gas-adsorbent.

Visualization of micro and nanostructures of the surfaces of powder particles and ceramics was carried out on scanning electron microscope (SEM) Zeiss Neon 40 EsB (Carl Zeiss, Germany). Insofar as the samples studied were dielectrics at room temperature, we covered them with a thin layer of platinum to prevent surface charging. The platinum layers 3 nm thick were deposited by means of spraying setup Leica EM SCD 500 (Leica Microsystems, Germany). Images were obtained at the accelerating voltage of 3 kV with detectors Inlens and SE2 (detection of secondary electrons) for the better topographical contrast. For better identification of materials, we used also ESB detector (detection of backscattered electrons).

Individual particles of nanopowders were studied by means of transmission electron microscope (TEM) LIBRA 200 (Carl Zeiss, Germany). For preparation of a sample, we placed a drop of aqueous suspension onto a Cu–C grid and dried in air.

Lamels of composite ceramics SDC + MgO were prepared and studied by means of electron microscope Crossbeam 540 SEM-FIB (Carl Zeiss, Germany).

The thermal expansion of ceramic samples was determined in the temperature interval of 23–868°C in air and in the nitrogen flow (50 mL/min) with the oxygen partial pressure of 1 Pa by means of a X-ray diffractometer NETZSCH DIL 402 C (Netzsch, Germany) and also based on X-ray diffraction by the shift of main peaks in X-ray patterns of the sample with the increase in the temperature in air.

Impedance of ceramic cuboids covered with platinum or silver on their opposite sides in the direction of current was measured on alternating current by means of measuring system IM6e (Impedance Measurement Unit) (Zahner-elektrik, GmbH and Co. KG, Germany) in the frequency range from 10 mHz to 1 MHz at the ac voltage of 15 mV. The measurements were carried out in the temperature interval of 20–850°C in air and in the flow of gas mixture $Ar/H_2/H_2O/O_2$ with $pH_2/pH_2O = 11$.

RESULTS AND DISCUSSION

Characterization of SDC Powder and Single-Phase Ceramics

The particle size of synthesized SDC nanopowders determined directly by means of transmission electron microscopy and indirectly by means of X-ray diffractometry by the method of Williamson–Hall [28] were estimated to be 10–30 nm. The specific surface of this powder measured by the BET method was 50 m^2/g. Nanoparticles in as prepared powders formed aggregates with the size of 100–250 nm (Fig. 3). Figure 4 shows that as the heat-treatment temperature increased above 1000 K, the size of particles considerably increased due to sintering.

X-ray diffraction patterns of nanopowders prepared in such a way suggest that the samples were single-phase and contained no visible inclusions of other compounds. As the temperature increased, the dif-

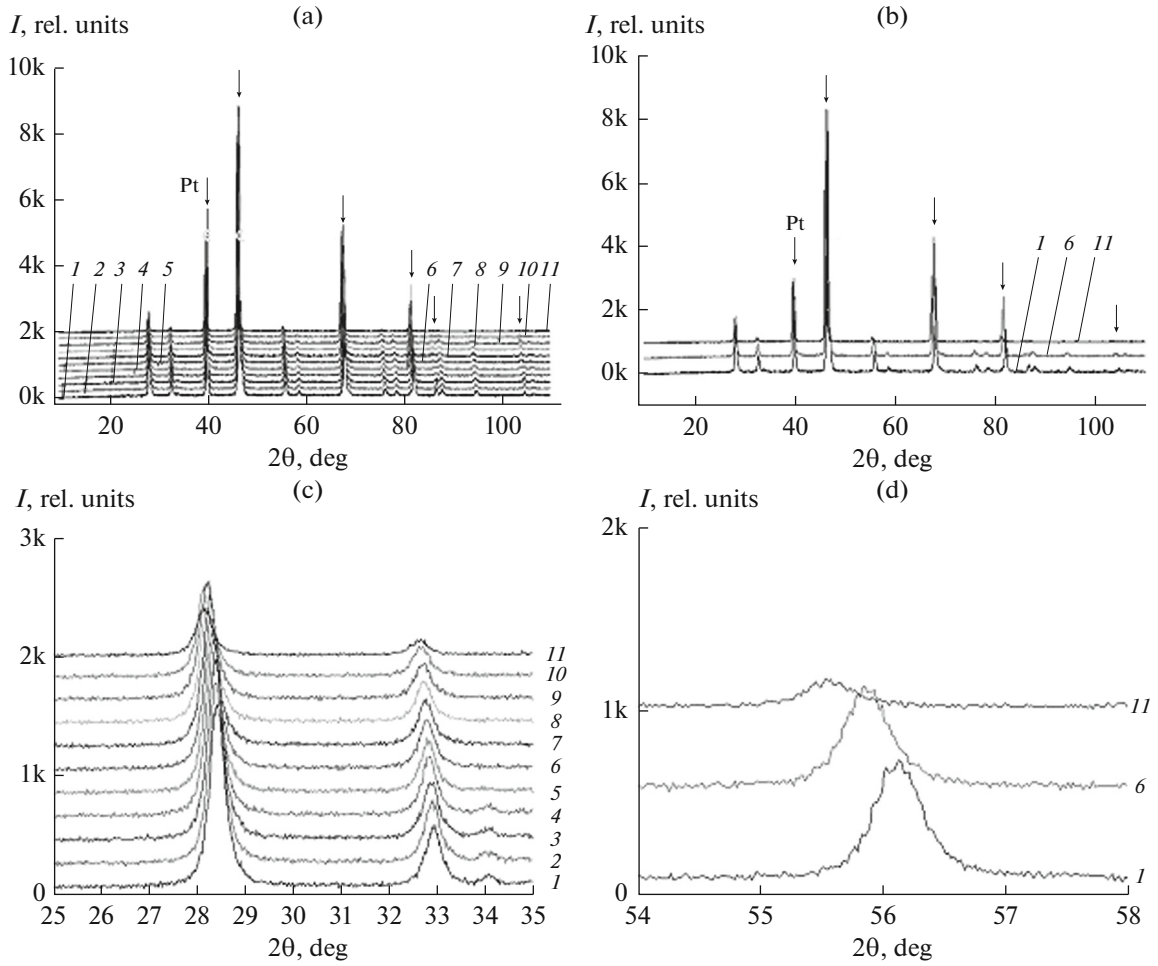

Fig. 5. X-ray diffraction patterns of $Ce_{0.8}Sm_{0.2}O_{1.9-\delta}$ nanoparticles recorded in 1×10^{-7} bar vacuum at different temperatures: (*1*) 25, (*2*) 100, (*3*) 200, (*4*) 300, (*5*) 400, (*6*) 500, (*7*) 600, (*8*) 700, (*9*) 800, (*10*) 900, (*11*) 1000°C; (a) and (b) are the angles pertaining to platinum at room temperature.

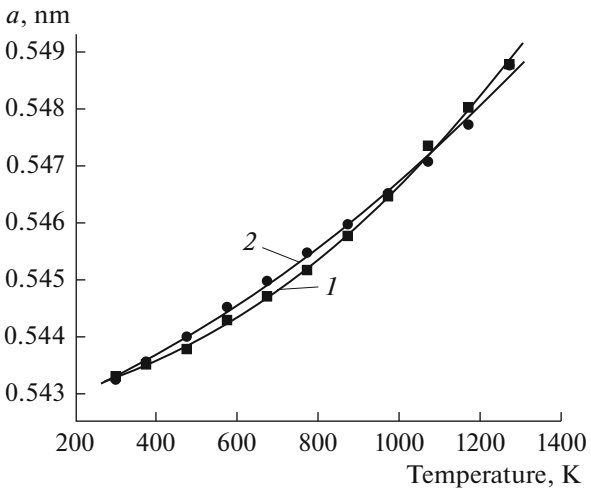

Fig. 6. Temperature dependence of lattice parameters of $Ce_{0.8}Sm_{0.2}O_{1.9-\delta}$ determined in (*1*) air and (*2*) in vacuum with the pressure of 1×10^{-7} bar.

fraction peaks were observed to shift to smaller angles, which pointed to the increase in the unit cell parameters of $Ce_{0.8}Sm_{0.2}O_{1.9-\delta}$ (Fig. 5). It is probable that the increase in the lattice parameter of this compound at the high temperature in vacuum of about 1×10^{-7} bar was associated not only with the thermal expansion but also with the change in the oxygen content in the material studied. This is confirmed by the data in Fig. 6, which shows the temperature dependences of *a* (nm) of the $Ce_{0.8}Sm_{0.2}O_{1.9-\delta}$ unit cell, determined by the position of peaks in diffraction patterns obtained in air and in vacuum of 1×10^{-7} bar. At temperatures above 1000 K, the lattice parameters determined in air are lower than those determined in vacuum, whereas above 1000 K the trend is the opposite. Such situation at temperatures above 1000 K could arise because the sample loses more oxygen in vacuum than in air. At the lower temperatures, the effect of pressure on the oxygen content in the material may be less pronounced.

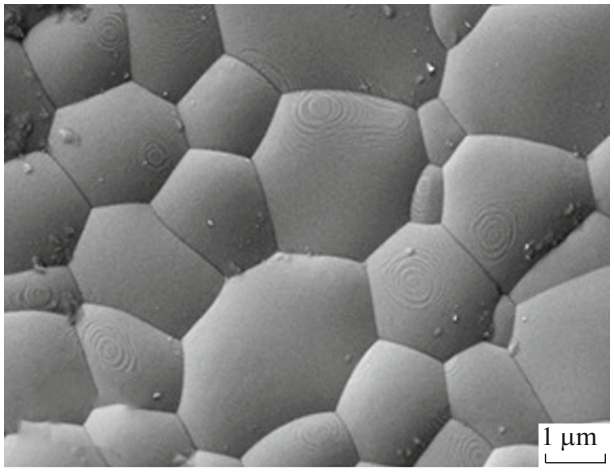

Fig. 7. Ceramics $Ce_{0.8}Sm_{0.2}O_{1.9}$ synthesized by 5 h sintering in air at temperature 1500°C.

Figure 7 shows the microstructure of single-phase ceramics prepared by pressing $Ce_{0.8}Sm_{0.2}O_{1.9}$ powder, followed by its 5 h sintering in air at 1500°C. It is evident that the size of the majority of particles of such ceramics varies from 500 to 5000 nm. On the surface of relatively coarse particles, surface relief is observed in the form of irregular circles. The elucidation of their origin was beyond the scopes of this study. The ceramic structure remained gas-tight both on the surface and in the bulk of samples.

Characterization of the Structure of Composite Ceramics SDC + MgO

For finer and more uniform distribution of particles of nanopowders of solid-electrolyte (SDC) and dielectric phases (MgO) throughout the composite ceramics, attempts were undertaken to use joint grinding of powders in planetary mill Pulverisette 7 in aqueous medium and ethanol and also the supersonic treatment of aqueous suspensions of these powder mixtures in supersonic mixer UIS250. Unfortunately, both methods failed to disintegrate the aggregated powder particles and after 5 h sintering at 1500°C the size of magnesium oxide inclusions in the composite ceramics remained within 500–5000 nm.

Considerable reduction in the particle size was achieved when preparing the (SDC + MgO) composite ceramics by the SHS method where the magnesium-containing compounds MgO or $Mg(NO_3)_2$ were introduced immediately into the initial glycine-citrate-nitrate mixture. The introduction of magnesium nitrate led to the most pronounced decrease in the size of component's particles. The size of magnesium oxide inclusions was of the order of magnitude of 100–1000 nm (Fig. 8). We observed the analogous situation earlier when synthesizing nanocomposite powders involving $Ce_{0.9}Gd_{0.1}O_{1.95}$ as the solid-electrolyte

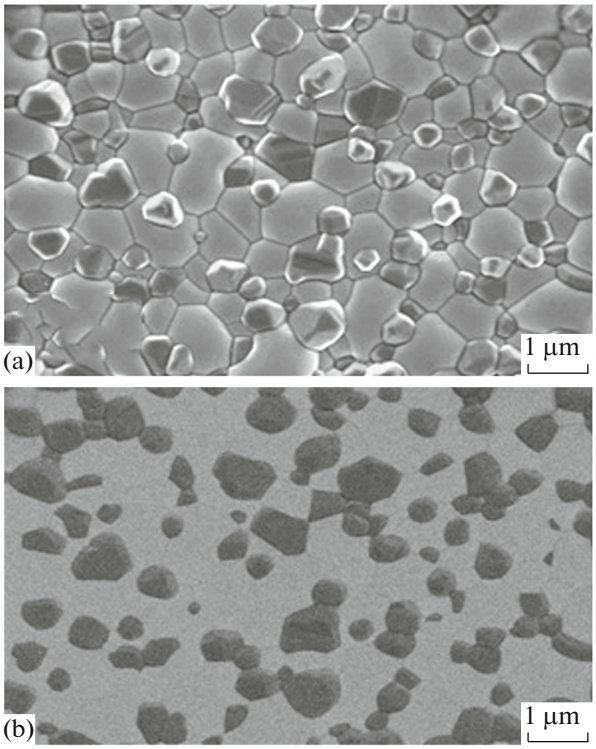

Fig. 8. SEM image of the surface of composite ceramics SDC + MgO prepared by sintering at 1500°C for 5 h: (a) InLens detector, (b) ESB detector.

phase and MgO as the dielectric phase: however, the size of magnesium oxide inclusions in this system [23] was approximately half their size in the system SDC + MgO.

To our regret we failed to obtain composite ceramics with a continuous network of grain boundaries $Ce_{0.8}Sm_{0.2}O_{1.9}$/MgO (SE/Ins). In terms of percolation theory [2], the so-called percolation threshold was not reached. Individual small clusters consisting of highly conductive grain boundaries SE/Ins failed to comprise the whole volume of the composite (Fig. 8). Apparently, to reach the percolation threshold it is necessary to optimize the component ratio, decrease the particle size, and increase the uniformity of their distribution throughout the ceramic material. Only then will small clusters coarsen, associate, absorb smaller clusters, and form the "infinite cluster" corresponding to the percolation threshold.

Figure 9 shows a structural fragment of the SDC + MgO composite ceramics from which is follows that at the interface between SDC and MgO, a certain film structure forms with the thickness of about 7.4 nm. This film has clear boundaries and the structure differing from both phases (SDC and MgO), which points to the limited mutual penetration of contacting components. The similar behavior of interfaces of adjacent phases was observed in [21] between YSZ film and MgO single crystal. The smaller thickness of

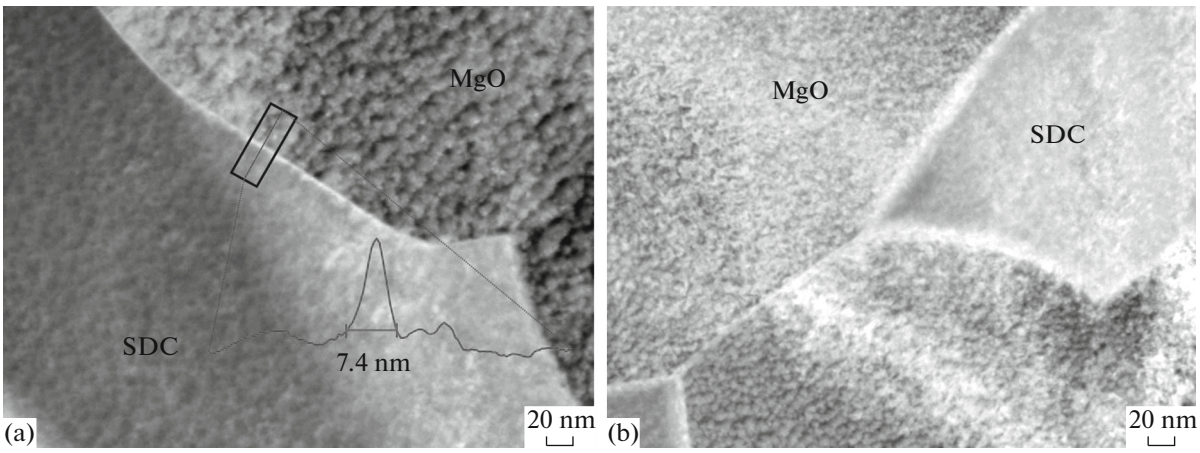

Fig. 9. SEM image of lamel of composite ceramics SDC + MgO sintered at 1600°C for 5 h. Insert in Fig. 9a shows the thickness of grain interface determined by changes in radiation intensity.

the boundary zone (1.6 nm) observed in [21] can be explained by the nature of solid electrolyte and different temperature of thermal treatment of contacting materials.

Thermal Expansion

On thermal cycling of the ceramic sample $Ce_{0.8}Sm_{0.2}O_{1.9}$ in air, the strictly reproducible relative thermal expansion was observed in the temperature interval of 23–850°C (Fig. 10, curves *1* and *2*). As we passed from air to the nitrogen flow, we observed the smaller expansion of samples as compared with air (curve *3*); subsequent cooling in the nitrogen flow was accompanied by considerable contraction of the sample as compared with air (curve *4*). Repeated thermal cycling in nitrogen flow led to still greater contraction of the sample (curves *5*, *6*), after which the form of curves was repeated on further cycling. The decrease in the sample size in the nitrogen flow with the lower oxygen content as compared with air is probably accompanied by the loss of a certain amount of oxygen within the homogeneity region of cerium-samarium oxide. This trend seems to be interesting, because for materials with perovskite and fluorite structure, the opposite trend was observed in studies of thermal expansion in air and gas media with the much lower oxygen concentration as compared with our experiments (10^{-11}–10^{-19} Pa), i.e., the decrease in the oxygen content within composition of perovskite-like compounds was accompanied by the increase in their unit cell [29–32]. Probably, the different character of lattice parameter variations is associated with the extent of oxygen nonstoichiometry. To obtain more detailed information on the effect of oxygen nonstoichiometry on the lattice parameter of $Ce_{0.8}Sm_{0.2}O_{1.9-\delta}$, additional studies should be carried out.

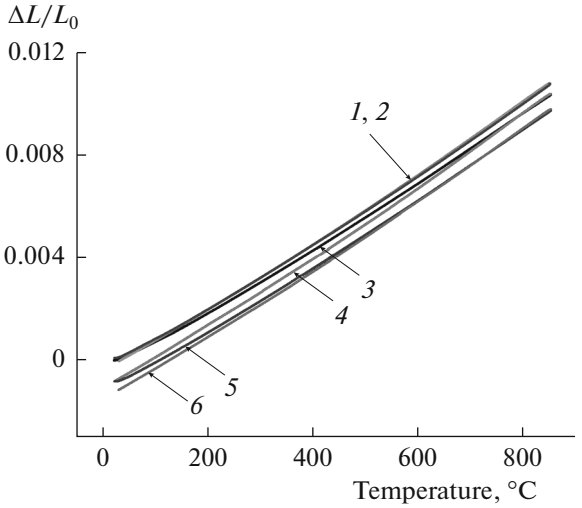

Fig. 10. Relative thermal expansion of ceramic sample $Ce_{0.8}Sm_{0.2}O_{1.9-\delta}$ during its heating-cooling in (*1*, *2*) air, (*3*) during its first subsequent heating in nitrogen flow, (*4*) during its first subsequent cooling in nitrogen flow, and (*5, 6*) and during subsequent repetition of thermal cycles (*3*, *4*) in nitrogen flow.

Conductivity

The simplest model describing the ionic transport through ceramic material assumes that the transport of electrically charged particles proceeds throughout bulk, boundaries, and free surface of grains. Solid ceramic electrolytes may be schematically represented as an ohmic resistance connected in series with one or two circuits involving an ohmic resistance and a capacitor connected in parallel [33–36].

Figures 11a and 11b illustrate a certain theoretical impedance spectrum and the possible equivalent circuit explaining the origin of this spectrum [37, 38].

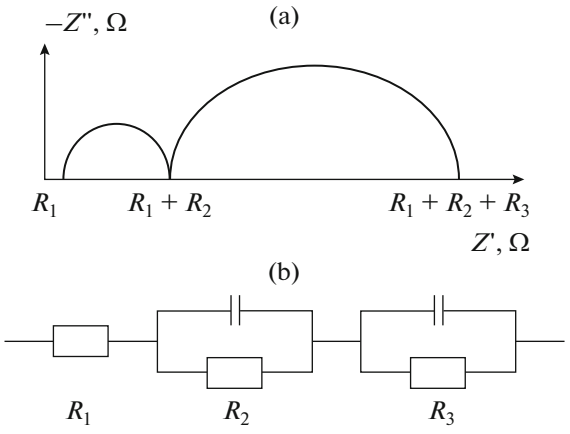

Fig. 11. Model explaining the origin of impedance spectra of single-phase solid-electrolyte ceramics: (a) impedance spectrum and (b) equivalent circuit for its theoretical simulation according to [37, 38].

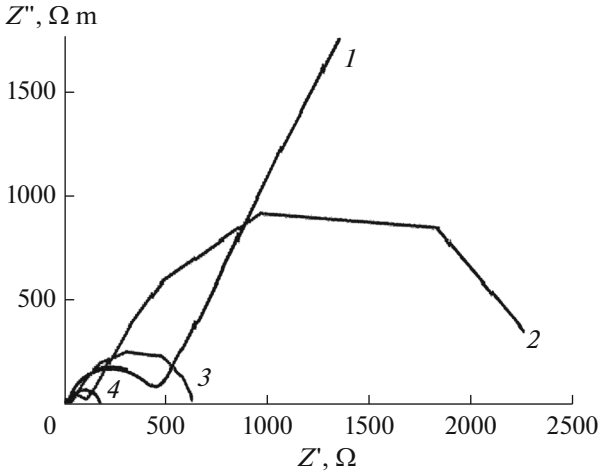

Fig. 12. Characteristic impedance spectra of the $Ce_{0.8}Sm_{0.2}O_{1.9-\delta}$ sample at different temperatures in air: (*1*) 600, (*2*) 700, (*3*) 800, and (*4*) 900°C.

According to [39], the resistances R_1 and R_2 in Fig. 11a correspond to bulk and grain-boundary resistances of solid-electrolyte materials and R_3 is the resistance of the electrode reaction.

Figure 12 shows typical impedance spectra of single-phase $Ce_{0.8}Sm_{0.2}O_{1.9}$ measured at different temperatures. It is seen that as the temperature increases, both bulk and grain-boundary conductivities of ceramics regularly increase. Figure 13 shows the total conductivity of single-phase (SDC) and nanocomposite (SDC + MgO) ceramics. The conductivity values found for single-phase (SDC) ceramics adequately agree with the data of [40]. The fact that the conductivity of single-phase SDC samples is a little lower as compared with [40] can be associated with the porosity of ceramics which was ignored in our study. As follows from Fig. 13, the introduction of 50 mol % of dielectric magnesium oxide into the composition of SDC ceramics had virtually no effect on the conductivity of composite ceramics SDC + MgO as compared with SDC ceramics. This result may be associated with the fact that in the composite ceramics containing a dielectric component in the form of magnesium oxide, regions appear with the conductivity higher as compared with the single-phase SDC ceramics. Taking into account the higher resistance of grain boundaries SDC/SDC as compared with the SDC volume [19, 20] and also the dielectric properties of MgO, the most probable factor for the retention of conductivity of composite ceramics after the addition of magnesium oxide should be the higher conductivity of SDC/MgO grain boundaries that appear in the structure of composite ceramics. To give the ultimate answer on the reasons for retention of conductivity of composite ceramics SDC + MgO as compared with single-phase SDC ceramics, the aforementioned additional investigations will be carried out soon aimed at development of a continuous network of SE/Ins grain boundaries in the ceramics structure. If the higher conductivity of SDC/MgO grain boundaries as compared with the volume of SDC grains is confirmed, then new prospects will appear for the development of composite ceramics in this system with the high fraction of grain boundaries within the composite material and, as a consequence, for the development of the oxide solid-electrolyte material with the higher conductivity.

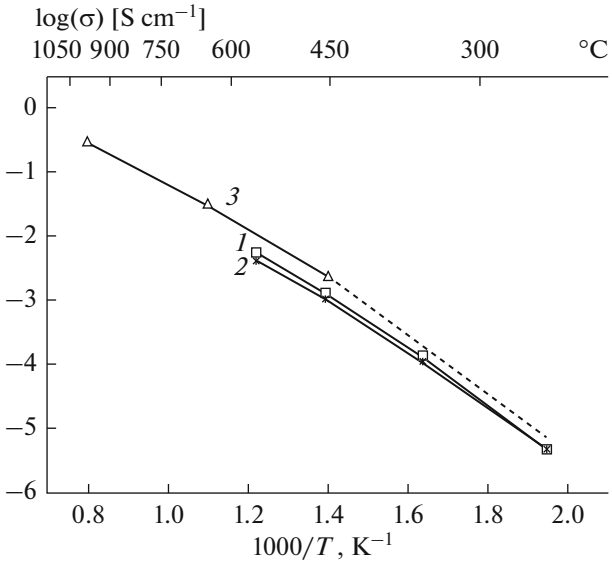

Fig. 13. Temperature dependence of conductivity of (*1*) SDC and (*2*) SDC : MgO = 1 : 1 samples measured in air as compared with (*3*) data of [40].

CONCLUSIONS

The studies of the phase composition, microstructure, thermal expansion, and conductivity of nanocomposite ceramics SDC + MgO provided grounds for the assumption that the latter contains additional routes for accelerated transport of oxygen ions as compared with single-phase ceramics SDC. These routes are localized along the boundaries between adjacent dielectric and solid-electrolyte phases. A model is proposed for calculating the conductivity of composite ceramics, which is based on the conductivity value and the grain size of components under the assumption that the grain boundary between components in the composite material has a certain thickness.

ACKNOWLEDGMENTS

We are grateful to H. Stegmann from the Zeiss microscopy laboratory in Oberkochen (Germany) and also to Nora Haufe from the Kurt-Schwabe-Institut für Mess- und Sensortechnik e.V. Meinsberg (Germany) for electron microscopic images shown in Figs. 9a, 9b and in Fig. 3, respectively.

This study was supported by the Ministry of Education and Research of Germany (project Oxeen–03EK3029C) and also by the Belarus State Program for Scientific Research "Chemical Technologies and Materials" (subprogram "New Chemical Technologies and Products," objective 2.1).

REFERENCES

1. Chebotin, V.N. and Perfilev, M.V., *Elektrokhimiya tverdykh elektrolitov* (Electrochemistry of Solid Electrolytes),Moscow: Khimiya, 1978 [in Russian].
2. Ivanov-Shits, A.K. and Murin, I.V., *Ionika tverdogo tela* (Solid State Ionics) Vol. 1, St. Petersburg: SPb Univ., 2010 [in Russian]
3. Ivanov-Shits, A.K., and Murin, I.V., *Ionika tverdogo tela* (Solid State Ionics) Vol. 2, St. Petersburg: SPb Univ., 2010 [in Russian].
4. Uvarov, N.F., *Kompositnye tverdye elektrolity* (Composite Solid Electrolytes), Novosibirsk: SO RAN, 2008) [in Russian].
5. Liang, C.C., Conduction characteristics of the lithium iodide-aluminum oxide solid electrolytes, *J. Electrochem. Soc.*, 1973, vol. 126, p. 1289.
6. Liang, C.C., US Patent H01M6/18, no. 3 713 897 (USA), 1973.
7. Uvarov, N.F., Isupov, V.P., Sharma, V., and Shukla, A.K., Effect of morphology and particle size on the ionic conductivities of composite solid electrolytes, *Solid State Ionics*, 1992, vol. 51, p. 41.
8. Uvarov, N.F., Bokhonov, B.B., Isupov, V.P., and Hairetdinov, E.F., Nanocomposite ionic conductors in the $LiSO_4$–Al_2O_3 system, *Solid State Ionics*, 1994, vol. 74, p. 15.
9. Chovdary, P., Tare, V.B., and Wagner, J.B., Electrical conduction in AgJ–Al_2O_3 composites, *J. Electrochem. Soc.*, 1985, vol. 132, p. 123.
10. Jow, T. and Wagner, J.B., The effect of dispersed alumina particles on the electrical conductivity of cuprous chloride, *J. Electrochem. Soc.*, 1979, vol.126, p. 1963.
11. Fujitsu, S., Miyayama, M., and Koumoto, K., Enhancement of ionic conduction in CaF_2 and BaF_2 by dispersion of Al_2O_3, *J. Mater. Sci.,* 1985, vol. 20, p. 2103.
12. Saito, Y. and Maier, J., Conductivity enhancement of CaF_2 by grain boundary activation with Lewis acids, *Solid State Ionics*, 1996, vol. 86–88, p. 581.
13. Guo, X. and Yuan, R-Z., Grain boundary ionic conduction of zirconia-based solid electrolyte: idea and practice, *Mat. Sci. Lett.*, 1995, vol. 14, p. 499.
14. Brosa, S., Bouwmeester, H.J.M., and Guth, U., Electrical conductivity and thermal behavior of solid electrolytes based on alkali carbonates and sulfates, *Solid State Ionics*, 1997, vol. 101–103, p. 1201.
15. Gauthier, M. and Chamberland, A., Solid-State detectors for the potentiometric determination of gaseous oxides: I. Measurement in air, *J. Electrochem. Soc.*, 1977, vol. 124, p. 1579.
16. Maier, J., Enhancement of the ionic conductivity in solid-solid-dispersions by surface induced defects, *Ber. Bunsen-Ges.*, 1984, vol. 88, p. 1057.
17. Meyer, C., Baumann, R., Günther, A., Vashook, V., Schmiel, T., Guth, U., and Fasoulas, S., Development of a solid state sensor for nitrogen oxides with a nitrate electrolyte, *Sens. Actuators, B*, 2013, vol. 181, p. 77.
18. Zhao, Y., Xia, C., Jia, L., Wang, Z., Li, H., Yu, J., and Li, Y., Recent progress on solid oxide fuel cell: Lowering temperature and utilizing non-hydrogen fuels, *Int. J. Hydrogen Energy,* 2013, vol. 38, p. 1649.
19. Kudo, T. and Ohayashi, H., Oxygen ion conduction of the fluorite-type $Ce_{1-x}Ln_x0_{2-x/2}$ (Ln = lanthanoid element), *J. Electrochem. Soc.*, 1975, vol. 122, p. 142.
20. Martin, M.C. and Mecartney, M.L., Grain boundary ionic conductivity of yttrium stabilized zirconia as a function of silica content and grain size, *Solid State Ionics,* 2003, vol. 161, p. 67.
21. Kosacki, I., Rouleau, Ch.M., Becher, P.F., Bentley, J., and Lowndes, D.H., Nanoscale effects on the ionic conductivity in highly textured YSZ thin films, *Solid State Ionics,* 2005, vol. 176. p. 1319.
22. Amosov, A.P., Borovinskaya, I.P., and Merganov, A.G., *Poroshkovaya tekhnologiya samorasprostranyayushchegosya vysokotemperaturnogo sinteza materialov, Uchebn. posobie* (Powder Technology of the Self-Propagating High-Temperature Synthesis of Materials. Manual), Antsiferov, V.N. (Ed.), Moscow: Mashinostroenie-1, 2007 [in Russian].
23. Vashook, V., Zosel, J., Sperling, E., Guth, U., and Mertig, M., Nanocomposite ceramics based on $Ce_{0.9}Gd_{0.1}O_{1.95}$ and MgO, *Solid State Ionics,* 2016, vol. 288, p. 98.
24. Banerjee, S., Sujatha Devi, P., Topwal, D., Mandal, S., and Menon, K., Enhanced ionic conductivity in $Ce_{0.8}Sm_{0.2}O_{1.9}$: Unique effect of calcium Co-doping, *Adv. Funct. Mater.* 2007, vol. 17, p. 2847.
25. Banerjee, S. and Sujatha Devi, P., Sinter-active nanocrystalline CeO_2 powder prepared by a mixed fuel process: Effect of fuel on particle agglomeration, *J. Nanopart. Res.,* 2007, vol. 9, p. 1097.

26. Banerjee, S. and Sujatha Devi, P., Understanding the effect of calcium on the properties of ceriaprepared by a mixed fuel process, *Solid State Ionics,* 2008, vol. 179, p. 661.
27. Basu, S., Sujatha Devi, P., and Maiti, H.S., Synthesis and properties of nanocrystalline ceria powders, *J. Mater. Res.,* 2004, vol. 19, p. 3162.
28. Williamson, G.K. and Hall, W.H., X-ray line broadening from filed aluminium and wolfram, *Acta Metall.,* 1953, vol. 1, p. 22.
29. Atkinson, A. and Ramos, T.M.G.M., Chemically-induced stresses in ceramic oxygen ion-conducting membranes, *Solid State Ionics,* 2000, vol. 129, p. 259.
30. Zuev, A.Yu., Vylkov, A.I., Petrov, A.N. and Tsvetkov, D.S., Defect structure and defect-induced expansion of undoped oxygen deficient perovskite $LaCoO_{3-\delta}$, *Solid State Ionics,* 2008, vol. 179, p. 1876.
31. Zuev, A.Yu., Petrov, AN., Vylkov, A.I., and Tsvetkov, D.S., Oxygen nonstoichiometry and defect structure of undoped and doped lanthanum cobaltites, *J. Mater. Sci.*, 2007, vol. 42, p. 1901.
32. Hayashi, H., Suzuki, M., and Inaba, H. Thermal expansion of Sr- and Mg-doped $LaGaO_3$, *Solid State Ionics,* 2000, vol. 128, p. 131.
33. Nadeem, M., Akhrar, M.J., and Khan, A.Y., Effects of low frequency near metal-insulator transition temperatures on polycrystalline $La_{0.65}Ca_{0.35}Mn_{1-y}Fe_yO_3$ (where $y = 0.05–0.10$) ceramic oxides, *Solid State Commun.,* 2005, vol. 134, p. 431.
34. Deleebeeck, L., Fournier, J. L., and Birss. V., Comparison of Sr-doped and Sr-free $La_{1-x}Sr_xMn_{0.5}Cr_{0.5}O_{3\pm\delta}$ SOFC anodes, *Solid State Ionics,* 2010, vol. 181, p. 1229.
35. Lee, Y.-K., Kin, J.-Y., Lee, Y.-K., Kim, I., Moon, H.-S., Park, J.-W., Jacobson, C.P., and Visco, S.J., Conditioning effects on $La_{1-x}Sr_xMnO_3$-yttria stabilized zirconia electrodes for thin-film solid oxide fuel cells, *J. Power Sources,* 2003, vol. 115, p. 219.
36. Ortiz-Vitoriano, N., Ruiz de Larramendi, I., Ruiz de Larramendi, J. I., Arriortua, M. I., and Rojo, T., Synthesis and electrochemical performance of $La_{0.6}Ca_{0.4}Fe_{1-x}Ni_xO_3$ ($x = 0.1$, 0.2, 0.3) material for solid oxide fuel cell cathode, *J. Power Sources,* 2009, vol. 192, p. 63.
37. Mauvy, F., Lalanne, C., Bassat, J.-M., Grenier, J.-C., Zhao, H., Huo, L., and Stevens, P., Electrode properties of Ln_2NiO_4: AC impedance and DC polarization studies, *J. Electrochem. Soc.,* 2006, vol. 153, p. A1547.
38. Ruiz de Larramendi, I., Ortiz, N., López-Antón, R., and Ruiz de Larramendi, J.I., Structure and impedance spectroscopy of $La_{0.6}Ca_{0.4}Fe_{0.8}Ni_{0.2}O_{3-\delta}$ thin films grown by pulsed laser deposition, *J. Power Sources,* 2007, vol. 171, p. 747.
39. Barsoukov, E. and Macdonald, J.R., Solid state devices, in *Impedance Spectroscopy – Theory, Experiment, and Applications*, 2nd ed., Hoboken: Wiley, 2005, ch. 4.3, p. 282.
40. Kudo, T. and Obayashi, H., Mixed electrical conduction in the fluorite-type $Ce_{1-x}Gd_xO_{2-x/2}$, *J. Electrochem. Soc.,* 1976, vol. 123, p. 415.

Translated by T. Safonova